

Searching for Domain Wall Network by Parkes Pulsar Timing Array

Ligong Bian,^{1,2,*} Shuailiang Ge,^{2,3,†} Changhong Li,⁴ Jing Shu,^{3,2,‡} and Junchao Zong^{5,6}

¹Department of Physics and Chongqing Key Laboratory for Strongly Coupled Physics, Chongqing University, Chongqing 401331, China

²Center for High Energy Physics, Peking University, Beijing 100871, China

³School of Physics and State Key Laboratory of Nuclear Physics and Technology, Peking University, Beijing 100871, China

⁴Department of Astronomy, Key Laboratory of Astroparticle Physics of Yunnan Province, School of Physics and Astronomy, Yunnan University, No.2 Cuihu North Road, Kunming, 650091 China

⁵Department of Physics, Nanjing University, Nanjing 210093, China

⁶CAS Key Laboratory of Theoretical Physics, Institute of Theoretical Physics, Chinese Academy of Sciences, Beijing 100190, China

We search for stochastic gravitational wave background generated by domain wall networks in the Data Release-2 of Parkes Pulsar Timing Array and find that the observed strong common power-law process can be explained by domain wall networks for the wall tension $\sigma_{\text{DW}} \sim (29 - 414 \text{ TeV})^3$ and the wall-decay temperature $T_d \sim 26 - 363 \text{ MeV}$. Interestingly, the same parameter region can largely alleviate the Hubble tension, if the free particles generated from domain wall networks further decay into dark radiation. In addition, the preferred parameter space corresponds to the axion mass range $m_a \sim 10^{-13} - 10^{-8} \text{ eV}$ for QCD axion. On the other hand, assuming that the common power-law process is not due to domain wall networks, we can put stringent constraints on the wall tension and decay temperature around the energy scale of QCD phase transition.

Introduction. A domain wall (DW) is a two-dimensional topological defect forming as a field connecting discrete vacua. In the early Universe, after symmetry breaking, different uncorrelated patches can choose different vacua and a highly-percolated DW network can form through the Kibble-Zurek mechanism [1, 2][62]. The dynamics of a DW network has nonzero quadrupole momentum and thus can generate gravitational waves (GWs), which numerical simulations have confirmed (see e.g., Refs. [3–5]). On the other hand, since DWs dilute slower than matter and radiation with cosmic expansion, they will finally dominate the Universe’s energy density. Therefore, they may lead to a picture contradictory to the present Universe, known as the DW problem [6]. One way to resolve this problem is to introduce a biased potential to break the vacua degeneracy so that the walls will quickly decay and disappear [7–9]. This is also the end of GW production. The magnitude and peak-frequency position of the produced GW spectrum are determined by the DW tension and the biased potential (equivalently, DW tension and the decay time). DW can arise in many prospective particle models featured with symmetry breaking(s) that can generate discrete vacua. For QCD axion model [10, 11], axion strings firstly form when the Peccei-Quinn symmetry spontaneously breaks (after inflation) as one of the most promising ways to solve the strong CP problem [10, 11]. During the QCD phase transition, axion string-wall network forms where strings play a minor role in GW production since DWs dominate the network dynamics due to their large wall tension [4, 12]. The stochastic GW background (SGWB) generated by DW networks falls into the detection frequency region of Pulsar Timing Array (PTA) experiments for certain parameter ranges.

PTA experiments are built to fulfill several science targets by monitoring millisecond pulsars (MSP) with the extremely precise time of arrivals (ToAs) accumulated over a long data span. Recently, strong evidence of a common power-law (CPL) process has been found in the analyses of NANOGrav 12.5 years data [13]. Later, it is confirmed by other PTA col-

laborations, e.g., Parkes Pulsar Timing Array (PPTA) [14] and European Pulsar Timing Array (EPTA) [15]. The finding of this CPL signal is quite encouraging since it is viewed as the first light of GW detection via PTA. However, the GW explanation for the CPL signal suffers from the lack of characteristic feature “Hellings-Downs” (HD) correlation, and the signal origin remains unknown which could either be a source or a systematic error. Nevertheless, to explain the CPL signal, many efforts have been paid to search for SGWB from many sources, such as supermassive black hole binaries (SMBHBs), first-order phase transitions, and cosmic strings, etc. [16–21]. The DW-induced SGWB is of broken power-law shape rather than of wide-frequency-range plateau shape as cosmic strings. In this work, we utilize the second dataset released by PPTA to search for such a signal [22]. We take the DW tension and the bias potential (or the DW decay time) as two free parameters when searching for the corresponding GW signals in PPTA data. We find that certain parameter space of the DW network can explain the CPL process observed in the PPTA data. We also find that, for the same parameter space, the observed Hubble tension can be significantly alleviated by assuming free particles (generated from the DW network) could further decay into dark relativistic species. This might represent a clue to a DW network that ever existed in the early Universe. On the other hand, to be conservative, if we treat the CPL process as an unknown background that is not due to a DW network, we can give stringent constraints on DW parameters correspondingly.

SGWB spectra from DW networks. The interaction between DWs is so efficient that their density after formation will soon saturate the requirement of causality, i.e., approximately one piece of DW per Hubble patch H^{-3} . The energy density of DW networks thus evolves with the scaling behavior $\rho_{\text{DW}}(t) \propto H(t)$, which has been found and confirmed in multiple numerical simulations [4, 5, 23–26]. The DW density is $\rho_{\text{DW}} = \mathcal{A} \sigma_{\text{DW}} H$ where σ_{DW} is the wall tension and \mathcal{A} is the area parameter. DW networks radiate GWs with the power

$P_{\text{GW}} \sim G\ddot{Q}_{ij}\ddot{Q}_{ij}$ where $Q_{ij} \sim \mathcal{A}\sigma_{\text{DW}}H^{-4}$ is the quadrupole momentum of the walls. Then the energy density of GWs can be expressed as $\rho_{\text{GW}} = \epsilon P_{\text{GW}}/H^{-3} = \epsilon G\mathcal{A}^2\sigma_{\text{DW}}^2$ where an efficiency parameter ϵ is introduced. \mathcal{A} and ϵ are constant with time in the scaling regime and can be determined by numerical simulations [4, 5].

To avoid the DW domination problem, we introduce a biased potential ΔV to quickly kill the networks [7–9] by breaking the degeneracy of vacua on the two sides of a wall. Such wall decay happens at $t_d \simeq \sigma_{\text{DW}}/\Delta V$ when the biased potential energy of a vacuum patch is comparable with the energy of boundary wall. This is the time that the GW radiation stops, which determines the peak frequency of the GW spectra, $f_p(t_d) \simeq H(t_d)$ [4, 5]. We assume that t_d is in the radiation-dominant era. Then, the peak frequency today is

$$f_p(T_0) \simeq 3.6 \times 10^{-9} \text{ Hz} \left[\frac{10.75}{g_*(T_d)} \right]^{1/12} \left(\frac{1 \text{ TeV}^3}{\sigma_{\text{DW}}} \right)^{1/2} \left(\frac{\Delta V}{1 \text{ MeV}^4} \right)^{1/2}, \quad (1)$$

where g_* is the effective degrees of freedom for energy. We then define the GW spectra as

$$\Omega_{\text{GW}}(f, T) \equiv \frac{1}{\rho_c} \frac{d\rho_{\text{GW}}(f, T)}{d \ln f}, \quad (2)$$

where $\rho_c = 3H^2/(8\pi G)$ is the critical density. The present GW spectra at peak frequency is thus

$$\begin{aligned} \Omega_{\text{GW}}(f_p, T_0)h^2 \\ \simeq 5.2 \times 10^{-20} \mathcal{A}^2 \tilde{\epsilon} \left[\frac{10.75}{g_*(T_d)} \right]^{1/3} \left(\frac{\sigma_{\text{DW}}}{1 \text{ TeV}^3} \right)^4 \left(\frac{1 \text{ MeV}^4}{\Delta V} \right)^2, \end{aligned} \quad (3)$$

where $\tilde{\epsilon} \equiv [d\epsilon/d \ln f]_{f=f_p}$.

TABLE I: Fitted power value P for $f > f_p$.

N_{DW}	2	3	4	5	6
P	-1.077	-0.972	-0.887	-0.807	-0.731

As known, the spectra of $f < f_p$ goes as $\sim f^3$ because of causality [27, 28]. For $f > f_p$, simulations show that the slope is close to $\sim f^{-1}$ but slightly depends on the “domain wall number” N_{DW} which is the number of vacua [4, 5][63]. Here, we directly fit for the slope-power P from the simulation result shown as Figure 6 in [4]. The fitted power values are summarized in Table I. We consider scenarios of $N_{\text{DW}} \geq 2$ since the $N_{\text{DW}} = 1$ string-wall network is unstable and would disappear immediately after their formation without significant GWs production [29]. The complete GW spectra can be parameterized as $\Omega_{\text{GW}}(f, T_0)h^2 = \Omega_{\text{GW}}(f_p, T_0)h^2 \times (f/f_p)^n$ where $n = 3$ for $f < f_p$ and $n = P$ for $f > f_p$.

Throughout this work, we take the parameters $\mathcal{A} = 1.2$, $\tilde{\epsilon} = 0.7$ [4, 5] and fix $g_*(T_d)$ at 10.75. In Fig. 1, we show the GW spectra for various values of σ_{DW} and ΔV with $N_{\text{DW}} = 2$ as an example, in comparison with the free-spectra searching results for the SGWB amplitude using the most updated PPTA dataset (2nd release). This plot tells the rough region of DW

parameters that the PPTA data is sensitive to. We are going to carry out detailed data analysis in the following sections.

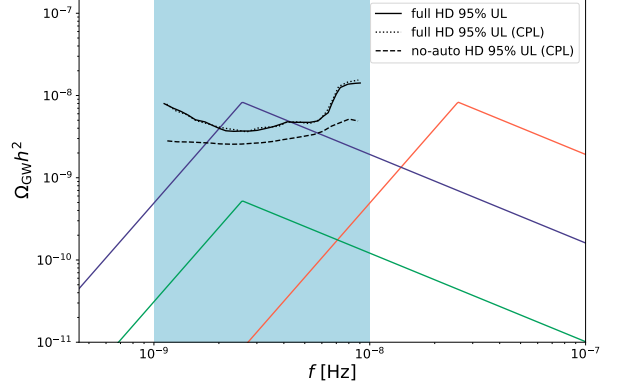


FIG. 1: The 95% upper limit (U.L.) on the SGWB amplitude by searching the most updated PPTA data. The shaded region indicates the PPTA sensitive frequency range. The black solid, dotted, and dashed lines are the search results under different hypotheses H2/3/4 in Table II (but with the DW spectra replaced by the free spectra in the corresponding hypotheses). We also show the GW spectra of $N_{\text{DW}} = 2$ as an example with different values of $(\log_{10} \sigma_{\text{DW}}/\text{GeV}^3, \log_{10} \Delta V/\text{GeV}^4)$: (16.3, -3.0) in red, (14.3, -7.0) in purple and (13.7, -7.6) in green for illustrative purpose.

Data Analysis. Our analyses use the second data release of the PPTA in the CSIRO pulsar data archive2 [64]. Following the standard procedure, we use the TEMPO2 tool [30, 31] to fit for the timing model of the pulsar arrays, the ENTERPRISE [65], ENTERPRISE_EXTENSIONS [66] and PTMCMCSampler [32] packages for the noise modeling and Bayesian analysis. The SGWB signal in PTA can be identified by searching for the HD correlation of ToAs of the pulsar array. Therefore, it is necessary to remove the noises generated from the observation. Generally, two kinds of noises need to be taken into account, the red and white noises. On one hand, red noises can arise from the irregular spin of the pulsars (spin noise) or the dispersion measure (DM) noise of the pulse when traveling through the interstellar media. On the other hand, for partial pulsars in the array, band noises will arise from the receiving of the single-frequency pulse. Specifically, there will be chromatic noises due to the receiving of chromatic frequency pulse on multiple bands. All kinds of red noises are modeled to have power-law spectra, parameterized by an amplitude A and a power γ . Then we use EFAC (Error FACTor) and EQUAD (Error added in QUADrature) to account for the additional white noise from the correlation of ToAs in multiple frequency channels, where the ToA uncertainties and ECORR (Error of CORrelation between ToAs in a single epoch) do not include. In practice, these white noise parameters are fixed by their maximum-likelihood values obtained from single pulsar analysis since they are barely related to SGWB model parameters [33]. All the parameters and their priors used in the Bayesian analysis are summarized in Table III in Appendix,

where we have also considered the constraints from e.g., big bang nucleosynthesis (BBN) to set the prior range of DW parameters.

Then, to extract signal information from posterior data, we adopt Bayesian analysis method here. We use the Bayes factor BF_{10} to measure the strength of the signal hypothesis H1 against the null hypothesis H0, which is given by the Savage Dickey formula[34]

$$\text{BF}_{10} = \frac{P_1(\mathbf{D})}{P_0(\mathbf{D})} = \frac{P(\phi = \phi_0)}{P(\phi = \phi_0 | \mathbf{D})}, \quad (4)$$

where $P_{0/1}(\mathbf{D})$ is the evidence of the noise/signal hypothesis with \mathbf{D} being the observational data. ϕ is the parameters of the signal model, and ϕ_0 is the values making the signal hypothesis null (for instance, the values that make the amplitude of SGWB signal vanish). By employing this formula, BF_{10} can be simply expressed by the ratio of the prior to the posterior probabilities of the null hypothesis. Note that the “null” and “signal” are relative concepts depending on the parameters we focus on.

We notice that Ref. [35] made a similar search by using both the NANOGrav 12.5 years datasets [36] (NG12) and the International PTA Data Release 2 [37] (IPTA DR2) datasets. Note that the PPTA DR2 we used in this work is independent of IPTA DR2. Besides, we also differ from them in the search strategies. Firstly, the SGWB spectra used here are directly interpreted from the result of the large field simulation [4], and we extract out the corresponding spectra for every single value of N_{DW} instead of treating it as a continuous parameter. By doing this, we can remove the uncertainty of one additional parameter in searching. It turns out that the searches in PPTA data yield similar results for $N_{\text{DW}} = 2$ to 6 DW networks. To be concise, in the following we present the result of $N_{\text{DW}} = 2$ case as a benchmark while leaving the details of $N_{\text{DW}} > 2$ results in Appendix. Secondly, we made the searches by using two different pairs of parameters as priors respectively: the wall tension σ_{DW} and the bias term ΔV and then with the second parameter replaced by the decay temperature T_d , and we will see they yield the consistent results. Then, we make a more thorough search including a) a direct search for the SGWB in the data with only white and red noises included, which yields the best-fit parameter values of DW; b) include or not include the auto-correlation between the pulsar pairs while taking the CPL as a systematic error, since the source of CPL still remains unknown; c) joint search for SGWB from the SMBHB and DW. As seen in [35], they only focused on parts a) and c). Besides, they set the HD overlap reduction function $\Gamma_{ab} = 1$ to simplify the computation while we adopt the strict formula to be conservative.

Results. To interpret PPTA data, we consider several typical hypotheses (labeled by Hn) which are summarized in Table II. H0 only includes the pulsar noise. H1 is to check the existence of a strong CPL signal. H2 is to search for a DW-induced SGWB signal with the full HD correlation included. Since the origin of the CPL signal is still not clear, we further consider hypotheses H3 and H4 where we add the CPL signal

as an unknown background in searching for a DW-induced SGWB signal. The difference between H3 and H4 is that H3 includes the full HD correlation while H4 only includes the off-diagonal (i.e., no-auto) HD correlation. In addition, we assume the CPL signal has an astrophysical origin, generated by SMBHBs. Analogous to H1 and H3, we get two new hypotheses, H5 and H6. In all cases, the Bayes ephemeris has been taken to include uncertainties from the solar system.

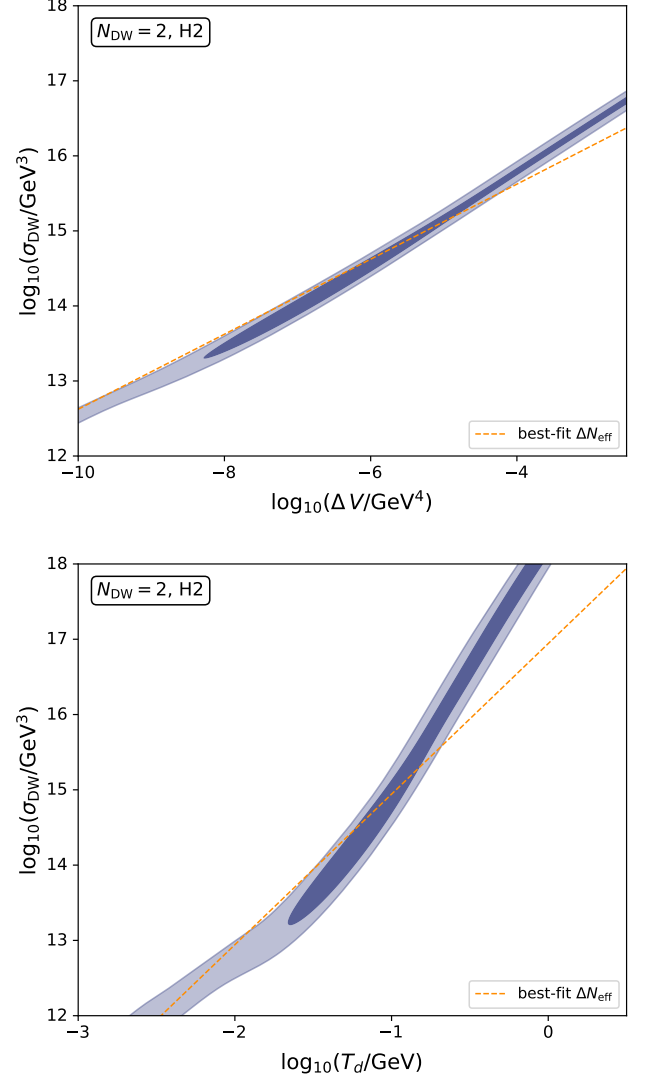


FIG. 2: Posterior distribution from the parameter combination of σ_{DW} and ΔV (Top), or σ_{DW} and T_d (Bottom) of $N_{\text{DW}} = 2$ for hypothesis H2 in Table II. 1 and 2- σ regions of the distribution are shown in light and dark colors. The orange dash line indicates the parameter region corresponding to the best-fit value of $\Delta N_{\text{eff}} = 0.151$.

First of all, a large Bayes factor $\text{BF}_{10} = 10^{3.2}$ of hypothesis H1 against H0 is found in our analyses, implying the existence of a strong CPL signal, which is consistent with PTA collaborations’ work [13–15]. We then test hypothesis H2 where the CPL process is replaced by the DW signal. We obtain a comparable Bayes factor of $\text{BF}_{20} = 10^{2.5}$ for the case

TABLE II: Description of the hypotheses, Bayes factors, and parameters estimation of $N_{\text{DW}} = 2$. “—” in the column of Parameters Estimation represents for the parameter is absent in that hypothesis.

Hypothesis	Pulsar Noise	CPL	SMBHB	DW Spectra	Parameter Estimation (68% C.L.)		
					$\log_{10} \Delta V / \text{GeV}^4, \log_{10} \sigma_{\text{DW}} / \text{GeV}^3$	$A_{\text{CPL}}, \gamma_{\text{CPL}}, A_{\text{SMBHB}} (\Delta V)$	Bayes Factors (ΔV)
					$\log_{10} T_d / \text{GeV}, \log_{10} \sigma_{\text{DW}} / \text{GeV}^3$	$A_{\text{CPL}}, \gamma_{\text{CPL}}, A_{\text{SMBHB}} (T_d)$	Bayes Factors (T_d)
H0	✓				—	—	—
H1	✓	✓			—	$-14.48^{+0.62}_{-0.64}, 3.34^{+1.37}_{-1.53}, \text{—}$	$10^{3.2} (/H0)$
H2	✓			✓(full HD)	$-6.21^{+2.59}_{-1.36}, 14.42^{+1.61}_{-0.76}$	—	$10^{2.5} (/H0)$
					$-1.10^{+0.66}_{-0.49}, 14.60^{+2.25}_{-1.20}$		$10^{2.7} (/H0)$
H3	✓	✓		✓(full HD)	$> -9.59, < 16.64$ (95% C.L.)	$-14.71^{+0.76}_{-1.51}, 3.16^{+1.63}_{-1.78}, \text{—}$	$0.86 (/H1)$
					$> -2.48, < 17.73$ (95% C.L.)	$-14.67^{+0.65}_{-0.98}, 3.42^{+1.47}_{-1.65}, \text{—}$	$0.98 (/H1)$
H4	✓	✓		✓(no-auto HD)	$> -9.62, < 16.32$ (95% C.L.)	$-12.53^{+0.14}_{-0.13}, 1.28^{+0.36}_{-0.36}, \text{—}$	$0.58 (/H1)$
					$> -2.54, < 17.75$ (95% C.L.)	$-13.62^{+0.14}_{-0.14}, 4.67^{+0.33}_{-0.32}, \text{—}$	$0.85 (/H1)$
H5	✓		✓		—	$\text{—}, \text{—}, -14.89^{+0.10}_{-0.12}$	$10^{3.3} (/H0)$
H6	✓		✓	✓(full HD)	$> -7.89, < 14.85$	$\text{—}, \text{—}, -14.94^{+0.13}_{-0.35}$	$0.70 (/H5)$
					$> -0.94, < 16.45$	$\text{—}, \text{—}, -14.92^{+0.11}_{-0.16}$	$0.90 (/H5)$

that σ_{DW} and ΔV are set as priors. Fitting results of the parameters at 68% Credential Level (C.L.) are listed in Table II: $\sigma_{\text{DW}} \sim (36\text{--}220 \text{ TeV})^3$ and $\Delta V \sim (13\text{--}124 \text{ MeV})^4$. As a comparison, we set σ_{DW} and T_d as priors in H2 and obtain consistent results: a Bayes factor of $\text{BF}_{20} = 10^{2.7}$ with the fitting results $\sigma_{\text{DW}} \sim (29\text{--}414 \text{ TeV})^3$ and $T_d \sim 26\text{--}363 \text{ MeV}$. The corresponding two-dimensional posterior distributions are shown in Fig. 2. The strip regions should be interpreted as the range of DW parameters that are preferred by PPTA data.

If PPTA data indeed shows the existence of a DW network based on the result of H2, we discuss the physical consequences in the following. In fact, GWs only carry a small portion of DW energy, while the free particles decayed from the walls carry most of the energy. Those particles behave as matter with momentum comparable with their mass, as shown by simulations [4]. To avoid the matter component (made of those free particles) dominating the Universe too early, we assume a simple scenario in this work that the free particles will further decay into dark radiation (DR) via their couplings with a dark sector (see e.g., Refs. [38–40]). More details are shown in Appendix. This process increases the effective number of relativistic species by ΔN_{eff} . By assuming the decay of free particles to dark radiation is instant after T_d (i.e., $\rho_{\text{DR}}(T_d) \simeq \rho_{\text{DW}}(T_d)$), we obtain $\Delta N_{\text{eff}} \simeq 0.083 \times [\sigma_{\text{DW}} / (10^{14} \text{ GeV}^3)]^2 \cdot [10^{-7} \text{ GeV}^4 / \Delta V]$. A more general expression of ΔN_{eff} is shown in Appendix. It is known that ΔN_{eff} can help resolve the Hubble tension, a 4.1σ tension between local and early-time measurements of the Hubble parameter H_0 [41–45]. It has been shown that the existence of self-interacting dark radiation, which might be achieved in our case via the coupling with the free particles or other new dark

couplings, can significantly reduce the Hubble tension to 2.7σ with the best-fit value $\Delta N_{\text{eff}} = 0.151$ [44, 46][67]. Then, using the above expression of ΔN_{eff} obtained in our scenario, we search for the parameter spaces of σ_{DW} , ΔV and T_d that give the best-fit values of ΔN_{eff} . The results are shown as the orange line in the two panels of Fig. 2. We see that the best-fit line largely overlaps with the parameter space preferred by PPTA data. Therefore, both the two observations, PPTA and Hubble tension, point to the same range of DW parameters. This might be a clue to the existence of a DW network in the early Universe which decayed around the temperature $T_d \sim 26\text{--}363 \text{ MeV}$.

On the other hand, if the strong CPL signal is not due to DWs, we can set constraints on the DW parameters. We find the Bayes factors for H3 and H4 against H1 are both less than 1, implying that the DW explanation is not favored by data when treating the CPL as a background. Again, we obtain consistent results by switching the priors to the group of σ_{DW} and T_d . See Table II for details. Correspondingly, we plot the 95% C.L. exclusion contours of the DW parameters in Fig. 3. Alternatively, we specify the unknown CPL signal as generated by SMBHBs. The Bayes factor for H6 against H5 is also less than 1. Both H6 and H3 give similar results as we can see from Table II and Fig. 3. This means that assuming a specific origin (SMBHB) for the CPL signal essentially does not affect setting exclusion regions for DW parameters.

In Fig. 3, we also show the existing constraint on DW parameters from the requirement that DWs should not overclose the Universe (see e.g., Ref. [47]). We see that the PPTA constraints are about one order of magnitude better than the existing one. To be more specific, the two-dimensional param-

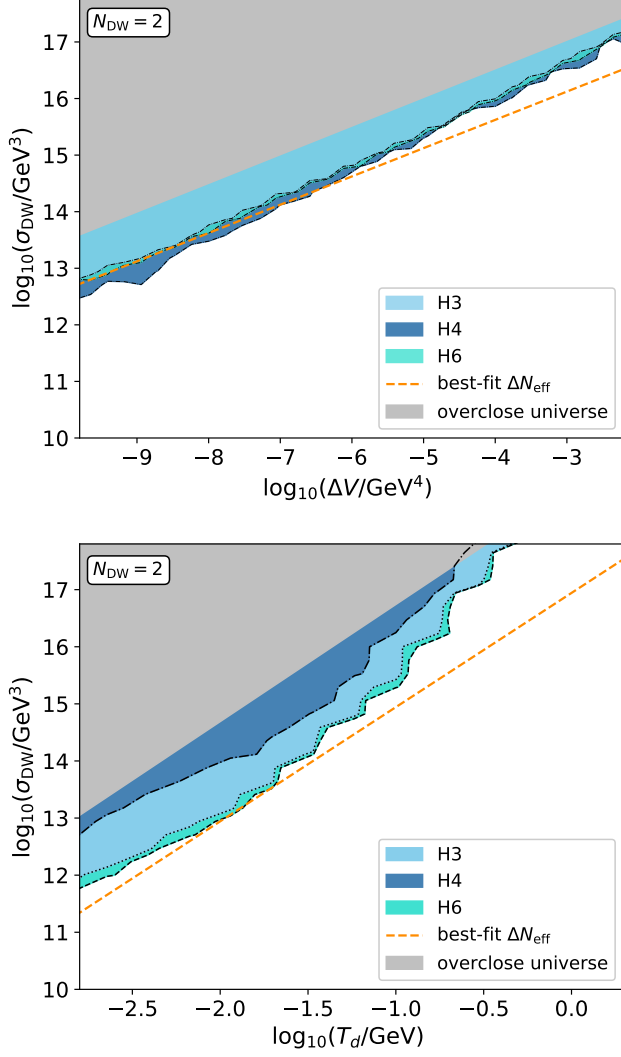


FIG. 3: 95% C.L. exclusion contour from the parameter combinations of σ_{DW} and ΔV (Top), or σ_{DW} and T_d (Bottom) of $N_{\text{DW}} = 2$ under hypothesis H3, H4 and H6 in Table II.

eter region $[\sigma_{\text{DW}}/(10^7 \text{ TeV}^3)]^2 \gtrsim [\Delta V/(10^8 \text{ MeV}^4)]$ is excluded by PPTA data in the PPTA sensitive range $\sigma_{\text{DW}} \sim (10^3 - 10^9) \text{ TeV}^3$ and $\Delta V \sim (10^2 - 10^{10}) \text{ MeV}^4$. Similarly, from the second panel of Fig. 3, we see that the excluded region is about $[\sigma_{\text{DW}}/(10^7 \text{ TeV}^3)] \gtrsim [T_d/(100 \text{ MeV})]^2$ in the PPTA sensitive range $T_d \sim (1 - 10^{2.5}) \text{ MeV}$.

Summary. We have used PPTA DR2 to conduct a detailed search for DW networks by looking for the SGWB signal. We find a strip region of the DW parameter space can fit quite well with the data and can be used to explain the unknown strong CPL signal: $\sigma_{\text{DW}} \sim (36 - 220 \text{ TeV})^3$ and $\Delta V \sim (13 - 124 \text{ MeV})^4$, or in terms of σ_{DW} and T_d : $\sigma_{\text{DW}} \sim (29 - 414 \text{ TeV})^3$ and $T_d \sim 26 - 363 \text{ MeV}$. Then, we explored the cosmological implication of the scenario that free particles, as the DWs' decay product, further convert to dark

radiation. Surprisingly, we find that the same parameter space of σ_{DW} , ΔV or T_d that explains PPTA data can also significantly alleviate the Hubble tension from the reported 4.1σ to a low level, 2.7σ . Therefore, a DW network (which decayed at T_d) in the early Universe might simultaneously account for the PPTA signal and the Hubble tension. This might represent a clue to a DW network that ever existed.

In addition, if interpreted in the QCD axion framework, the parameter space preferred by PPTA data corresponds to the axion mass: $m_a \sim 10^{-13} - 10^{-8} \text{ eV}$. We have used $\sigma_{\text{DW}} \simeq 9.23 f_a^2 m_a$ [4] and also the fixed relation between m_a and the symmetry breaking scale in QCD axion models [48] for interpreting. Many terrestrial experiments aim to directly search for axions in this mass range, such as ABRACADABRA [49, 50], DM-Radio [51], SRF [52], WISPLC [53], SHAFT [54], and CASPER [55]. Searching for GW signal induced by the (axionic) DW network in PPTA data could be a cross-check and complementary to these experiments.

On the other hand, to be conservative, we test more hypotheses, e.g., including the CPL process as an unknown background, and then assuming the CPL process from an astrophysical source of SMBHB. In these cases, we found no significant evidence for DWs, and the following parameter space near the energy scale of QCD phase transition is excluded at 95% C.L.: $[\sigma_{\text{DW}}/(10^7 \text{ TeV}^3)]^2 \gtrsim [\Delta V/(10^8 \text{ MeV}^4)]$ and $[\sigma_{\text{DW}}/(10^7 \text{ TeV}^3)] \gtrsim [T_d/(100 \text{ MeV})]^2$ in the PPTA sensitive range $T_d \sim (1 - 10^{2.5}) \text{ MeV}$. This result can also set constraints on the axion mass range depending on the QCD phase transition dynamics. Furthermore, our results suggest that the discrepancy between the networks with different N_{DW} remains insignificant. More observation data in the future of the worldwide PTA and further independent large-scale simulation of DW networks will be helpful.

Acknowledgements-

L.B. is supported by the National Key Research and Development Program of China under Grant No. 2021YFC2203004, the National Natural Science Foundation of China (NSFC) under Grants No. 12075041 and No. 12147102, the Fundamental Research Funds for the Central Universities of China under Grants No. 2021CDJQY-011 and No. 2020CDJQY-Z003, and Chongqing Natural Science Foundation under Grant No. cstc2020jcyj-msxmX0814. S.G. is supported by the International Postdoctoral Exchange Fellowship Program and the Boya Postdoctoral Fellowship of Peking University. C.L. is supported by the NSFC under Grants No.11963005, and No. 11603018, by Yunnan Provincial Foundation under Grants No.2016FD006 and No.2019FY003005, by Reserved Talents for Young and Middle-aged Academic and Technical Leaders in Yunnan Province Program, by Yunnan Provincial High level Talent Training Support Plan Youth Top Program, and by the NSFC under Grant No.11847301 and by the Fundamental Research Funds for the Central Universities under Grant No. 2019CDJDWL0005. J.S. is supported by Peking University under startup Grant No. 7101302974 and the National Natural Sci-

ence Foundation of China under Grants No. 12025507, No. 12150015, No.12047503; and is supported by the Strategic Priority Research Program and Key Research Program of Frontier Science of the Chinese Academy of Sciences under Grants No. XDB21010200, No. XDB23010000, and No. ZDBS-LY-7003 and CAS project for Young Scientists in Basic Research YSBR-006.

Appendix

Parameters summary

The prior distributions and descriptions of the parameters of DW, PTA noise models, and SGWB model are summarized in Table III.

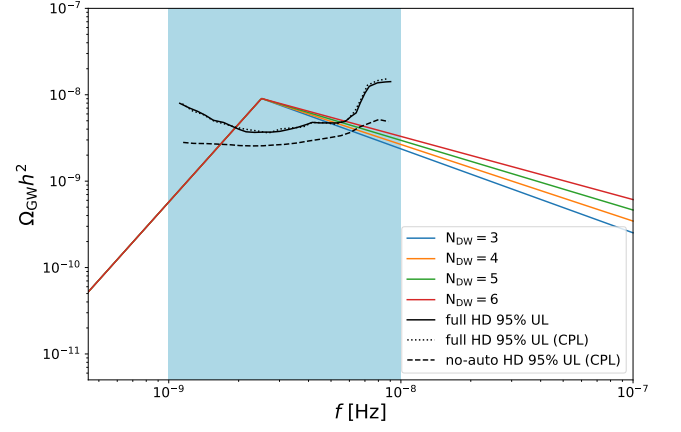


FIG. 4: Same as Fig. 1, but for $N_{\text{DW}} \geq 2$ cases. Also, the parameters are fixed at $(\log_{10} \sigma_{\text{DW}}/\text{GeV}^3, \log_{10} \Delta V/\text{GeV}^4) = (14.3, -7.0)$ for illustrative purpose.

Results from other hypotheses

DWs with $N_{\text{DW}} > 2$ are also considered in our model, and we here list the search results for $N_{\text{DW}} = 3, 4, 5$ and 6. First, we show the GW spectra corresponding to these N_{DW} values along with the free-spectra search of the SGWB amplitude in Fig. 4. Then, for each N_{DW} , we repeat the procedure of data analysis as done for the $N_{\text{DW}} = 2$ case. We summarize the detailed components of every hypothesis, the $1\text{-}\sigma$ regions of parameters, and the Bayes factor between different hypotheses in Table IV. Figs. 5, 7, 9, 11 show the posterior distributions of the parameters ΔV and σ_{DW} in different hypotheses described in the table, corresponding to the cases of the four N_{DW} values. (Results for the T_d case are shown in Figs. 6, 8, 10, 12). As can be seen, DW networks with $N_{\text{DW}} > 2$ can also offer a good explanation for the strong CPL process, with the Bayes factors of H2 ranging from $10^{1.8}$ to $10^{2.8}$ against the null hypothesis H0. Moreover, results similar to the $N_{\text{DW}} = 2$ case also arise when we include the CPL process as a background component, no matter whether we maintain the auto-correlation between the pulsars or consider the CPL process as an astrophysical source from the SMBHB. The Bayes factors are all distributed around 1, meaning a disfavoured evidence for H3/4/6 against H1. It might be helpful to distinguish between

TABLE III: Parameters and their prior distribution in data analysis. U and log-U stand for the uniform and log-uniform distribution.

parameter	Description	Prior	Comments
Noise parameters(θ)			
EFAC	White-noise modifier per backend	U [0, 10]	Fixed for setting limits
EQUAD	Quadratic white noise per backend	log-U [-10, -5]	Fixed for setting limits
ECORR	Correlated-ToAs white noise per backend	log-U [-10, -5]	Fixed for setting limits
A_{SN}	Spin-noise amplitude	log-U [-20, -6] (search) U [10^{-20} , 10^{-6}] (limit)	One parameter per pulsar
γ_{SN}	Spin-noise spectral index	U [0, 10]	One parameter per pulsar
A_{DM}	DM-noise amplitude	log-U [-20, -6] (search) U [10^{-20} , 10^{-6}] (limit)	One parameter per pulsar
γ_{DM}	DM-noise spectral index	U [0, 10]	One parameter per pulsar
A_{BAND}	Band-noise amplitude	log-U [-20, -6] (search) U [10^{-20} , 10^{-6}] (limit)	One parameter partial pulsars
γ_{BAND}	Band-noise spectral index One parameter per pulsar	U [0, 10]	One parameter partial pulsars
A_{CHROM}	Chromatic-noise amplitude	log-U [-20, -6] (search) U [10^{-20} , 10^{-6}] (limit)	One parameter partial pulsars
γ_{CHROM}	Chromatic-noise spectral index	U [0, 10]	One parameter partial pulsars
n_{CHROM}	Index of chromatic effects	U [0, 6]	Fixed for single pulsar
A_{CPL}	CPL process amplitude	log-U [-18, -11] (search) U [10^{-18} , 10^{-11}] (limit)	One parameter per PTA
γ_{CPL}	CPL process power index	U [0, 7]	One parameter per PTA
DW networks signal parameters (ψ)			
N_{DW}	DW number	[2, 3, 4, 5, 6] (fixed for each search)	One parameter per PTA
$\Delta V[\text{GeV}^4]$	Bias term	log-U [-10, -2] (search) U [10^{-10} , 10^{-2}] (limit)	One parameter per PTA
$\sigma_{\text{DW}}[\text{GeV}^3]$	Wall tension	log-U [10, 18] (search) U [10^{10} , 10^{18}] (limit)	One parameter per PTA
$T_d[\text{GeV}]$	Decay temperature	log-U [-3, 5] (search) U [10^{-3} , 10^5] (limit)	One parameter per PTA
BayesEphem parameters (ϕ)			
z_{drift}	Drift-rate of Earth's orbit about ecliptic z-axis	U [-10^{-9} , 10^{-9}] rad yr $^{-1}$	One parameter per PTA
$\Delta M_{\text{Jupiter}}$	Perturbation of Jupiter's mass	$N(0, 1.5 \times 10^{-11}) M_{\odot}$	One parameter per PTA
ΔM_{Saturn}	Perturbation of Saturn's mass	$N(0, 8.2 \times 10^{-12}) M_{\odot}$	One parameter per PTA
ΔM_{Uranus}	Perturbation of Uranus' mass	$N(0, 5.7 \times 10^{-11}) M_{\odot}$	One parameter per PTA
$\Delta M_{\text{Neptune}}$	Perturbation of Neptune's mass	$N(0, 7.9 \times 10^{-11}) M_{\odot}$	One parameter per PTA
PCA_i	Principal components of Jupiter's orbit	U [-0.05, 0.05]	One parameter per PTA

DW networks with different N_{DW} values, with more observation data coming in the near future, but we can only give the constraints on the parameters for now. The 1- σ C.L. limits of these parameters are all listed in Table IV.

To be complementary, we also reproduce the strong CPL signal using hypothesis H1. The CPL spectrum used in this paper is represented by

$$S(f) = \frac{A_{\text{CPL}}}{12\pi^2} \left(\frac{f}{\text{yr}^{-1}} \right)^{-\gamma_{\text{CPL}}} \text{yr}^3. \quad (5)$$

We obtain a 1- σ region for the amplitude and spectra index: $\log_{10} A_{\text{CPL}} = -14.48^{+0.62}_{-0.64}$ and $\gamma_{\text{CPL}} = 3.34^{+1.37}_{-1.53}$ with the Bayes factor of $\text{BF} = 10^{3.2}$. Then we made a trial to explain the

CPL signal by using the solely SMBHB process (H5), and it turned out to be a good explanation with a large Bayes factor, $\text{BF} = 10^{3.3}$, against the null hypothesis H0. The posterior distribution for $\log_{10} A_{\text{SMBHB}}$ is shown in Fig. 13. Then we also give the 1- σ region of the amplitude: $\log_{10} A_{\text{SMBHB}} = -14.89^{+0.10}_{-0.12}$. Note that the SGWB spectrum from the SMBHB used in this work is given by:

$$S(f) = \frac{A_{\text{SMBHB}}}{12\pi^2} \left(\frac{f}{\text{yr}^{-1}} \right)^{-\gamma_{\text{SMBHB}}} \text{yr}^3. \quad (6)$$

In this case, γ_{SMBHB} is fixed at 13/3, and A_{SMBHB} is assumed to take the prior distribution of log-U [-18, -14].

The domain wall networks and ΔN_{eff}

DW network can release its energy into two forms: GWs and free particles (i.e., axions or scalar particles) that build the walls, with the quantitative relation $\rho_{\text{GW}}/\rho_{\text{DW}} = 3/(8\pi) \cdot \epsilon \cdot \rho_{\text{DW}}/\rho_c$. Taking the typical values $\sigma_{\text{DM}} = 10^{14} \text{ GeV}^3$ and $\Delta V = 10^{-7} \text{ GeV}^4$ (thus $T_d \sim 20 \text{ MeV}$), we get $\rho_{\text{GW}}/\rho_c \sim 10^{-5}$ and $\rho_{\text{DW}}/\rho_c \sim 10^{-2}$ at T_d , which means that most of the energy is released into free particles. Furthermore, simulations show that those particles behave as cold matter with momentum comparable to the mass [4]. Consequently, for the parameter space we are interested in, such cold matter can dominate the Universe too early, which contradicts cosmological observations. Here, we consider one simple solution: those free particles can further decay into dark relativistic species (i.e., dark radiation, DR) via their couplings with a dark sector [38–40]. In this picture, free particles decay and inject energy into the dark radiation. It causes an increase in the effective number of relativistic species, $\Delta N_{\text{eff}} \equiv \rho_{\text{DR}}/\rho_{\nu}^{\text{SM}}$ where ρ_{ν}^{SM} is the energy density of (a single flavor) standard model neutrinos. A model-independent calculation shows that our scenario gives

$$\Delta N_{\text{eff}} \simeq \left(\frac{4}{11}\right)^{-\frac{4}{3}} \cdot \frac{4}{7} \cdot \frac{\rho_{\text{DW}}(T_d)}{\rho_c(T_d)} g_{*s}^{4/3}(T) g_{*s}^{-1/3}(T_d) \cdot F(\Gamma), \quad (7)$$

with $F(\Gamma) = \int_{t_d}^t \frac{a(t')}{a(t_d)} e^{-\Gamma(t'-t_d)} \Gamma dt'$.

g_{*s} is the effective degree of freedom for entropy. Γ is the decay rate from free particles to dark radiation. We require a large Γ to complete the decay before the BBN epoch $\sim 1 \text{ MeV}$ to avoid the potential violation of BBN observations. If Γ is sufficiently large ($\Gamma \gg t_d^{-1}$), $F(\Gamma) \simeq 1$ which returns to the case discussed in Ref. [35]. Furthermore, we expect that if the decay is not instant, in addition to alleviating the Hubble tension with the dark radiation, the residual free particles can also serve as dark matter. One can find various examples of such no-instant decay processes, for instance, in Ref. [56]). This issue is worthy of further study.

* Electronic address: lgbycl@cqu.edu.cn

† Electronic address: sge@pku.edu.cn

‡ Electronic address: jshu@pku.edu.cn

- [1] T. W. Kibble, *Journal of Physics A: Mathematical and General* **9**, 1387 (1976).
- [2] W. H. Zurek, *Nature* **317**, 505 (1985).
- [3] M. Kawasaki and K. Saikawa, *Journal of Cosmology and Astroparticle Physics* **2011**, 008 (2011).
- [4] T. Hiramatsu, M. Kawasaki, K. Saikawa, and T. Sekiguchi, *Journal of Cosmology and Astroparticle Physics* **2013**, 001 (2013), ISSN 1475-7516, 1207.3166, URL <https://iopscience.iop.org/article/10.1088/1475-7516/2013/01/001>.
- [5] T. Hiramatsu, M. Kawasaki, and K. Saikawa, *Journal of Cosmology and Astroparticle Physics* **2014**, 031 (2014), ISSN

- 1475-7516, 1309.5001, URL <https://iopscience.iop.org/article/10.1088/1475-7516/2014/02/031>.
- [6] Y. B. Zel'dovich, I. Y. Kobzarev, and L. B. Okun, *Zh. Eksp. Teor. Fiz.* **40**, 3 (1974).
- [7] P. Sikivie, *Physical Review Letters* **48**, 1156 (1982).
- [8] G. B. Gelmini, M. Gleiser, and E. W. Kolb, *Physical Review D* **39**, 1558 (1989).
- [9] S. E. Larsson, S. Sarkar, and P. L. White, *Physical Review D* **55**, 5129 (1997).
- [10] R. D. Peccei and H. R. Quinn, *Phys. Rev. Lett* **38**, 328 (1977).
- [11] R. D. Peccei and H. R. Quinn, *Physical Review D* **16**, 1791 (1977).
- [12] P. Sikivie, in *Axions* (Springer, 2008), pp. 19–50.
- [13] Z. Arzoumanian et al. (NANOGrav), *Astrophys. J. Lett.* **905**, L34 (2020), 2009.04496.
- [14] B. Goncharov et al., *Astrophys. J. Lett.* **917**, L19 (2021), 2107.12112.
- [15] S. Chen et al., *Mon. Not. Roy. Astron. Soc.* **508**, 4970 (2021), 2110.13184.
- [16] L. Bian, R.-G. Cai, J. Liu, X.-Y. Yang, and R. Zhou, *Phys. Rev. D* **103**, L081301 (2021), 2009.13893.
- [17] X. Xue et al., *Phys. Rev. Lett.* **127**, 251303 (2021), 2110.03096.
- [18] L. Bian, J. Shu, B. Wang, Q. Yuan, and J. Zong (2022), 2205.07293.
- [19] Z. Arzoumanian et al. (NANOGrav), *Phys. Rev. Lett.* **127**, 251302 (2021), 2104.13930.
- [20] N. Yonemaru et al., *Mon. Not. Roy. Astron. Soc.* **501**, 701 (2021), 2011.13490.
- [21] Z.-C. Chen, Y.-M. Wu, and Q.-G. Huang (2022), 2205.07194.
- [22] M. Kerr, D. J. Reardon, G. Hobbs, R. M. Shannon, R. N. Manchester, S. Dai, C. J. Russell, S. Zhang, W. van Straten, S. Osłowski, et al., *Publications of the Astronomical Society of Australia* **37** (2020), URL <https://doi.org/10.1017/2Fpsa.2020.11>.
- [23] W. H. Press, B. S. Ryden, and D. N. Spergel, *The Astrophysical Journal* **347**, 590 (1989).
- [24] B. S. Ryden, W. H. Press, and D. N. Spergel, *The Astrophysical Journal* **357**, 293 (1990).
- [25] T. Garagounis and M. Hindmarsh, *Physical Review D* **68**, 103506 (2003).
- [26] A. Leite, C. Martins, and E. Shellard, *Physics Letters B* **718**, 740 (2013).
- [27] C. Caprini, M. Chala, G. C. Dorsch, M. Hindmarsh, S. J. Huber, T. Konstandin, J. Kozaczuk, G. Nardini, J. M. No, K. Rummukainen, et al., *Journal of Cosmology and Astroparticle Physics* **2020**, 024 (2020), URL <https://doi.org/10.1088/1475-7516/2020/03/024>.
- [28] C. Caprini, R. Durrer, T. Konstandin, and G. Servant, *Physical Review D* **79**, 083519 (2009).
- [29] S. M. Barr, K. Choi, and J. E. Kim, *Nucl. Phys. B* **283**, 591 (1987).
- [30] G. Hobbs, R. Edwards, and R. Manchester, *Mon. Not. Roy. Astron. Soc.* **369**, 655 (2006), astro-ph/0603381.
- [31] R. T. Edwards, G. B. Hobbs, and R. N. Manchester, *Mon. Not. Roy. Astron. Soc.* **372**, 1549 (2006), astro-ph/0607664.
- [32] J. Ellis and R. van Haasteren, *jellis18/ptmcmcsampler: Official release* (2017), URL <https://doi.org/10.5281/zenodo.1037579>.
- [33] B. Goncharov et al., *Mon. Not. Roy. Astron. Soc.* **502**, 478 (2021), 2010.06109.
- [34] J. M. Dickey, *The Annals of Mathematical Statistics* **42**, 204 (1971), ISSN 00034851, URL <http://www.jstor.org/stable/2958475>.
- [35] R. Z. Ferreira, A. Notari, O. Pujolas, and F. Rompineve (2022),

TABLE IV: Description of the hypotheses, Bayes factors, and parameters estimation of $N_{\text{DW}} > 2$.

Hypothesis	Pulsar Noise	CPL	SMBHB	DW Spectra	Parameter Estimation (68% C.L.)		
					$\log_{10} \Delta V / \text{GeV}^4, \log_{10} \sigma_{\text{DW}} / \text{GeV}^3$	$A_{\text{CPL}}, \gamma_{\text{CPL}}, A_{\text{SMBHB}} (\Delta V)$	Bayes Factors (ΔV)
					$\log_{10} T_d / \text{GeV}, \log_{10} \sigma_{\text{DW}} / \text{GeV}^3$	$A_{\text{CPL}}, \gamma_{\text{CPL}}, A_{\text{SMBHB}} (T_d)$	Bayes Factors (T_d)
H0	✓				—	—	—
H1	✓	✓			—	$-14.48^{+0.62}_{-0.64}, 3.34^{+1.37}_{-1.53}, \text{—}$	$10^{3.2} (/H0)$
H2	$N_{\text{DW}} = 3$	✓		✓(full HD)	$-6.14^{+2.60}_{-1.48}, 14.47^{+1.61}_{-0.83}$ $-1.20^{+0.70}_{-0.64}, 14.31^{+2.29}_{-1.35}$	—	$10^{2.4} (/H0)$ $10^{2.6} (/H0)$
	$N_{\text{DW}} = 4$	✓		✓(full HD)	$-6.08^{+2.63}_{-1.54}, 14.50^{+1.65}_{-0.86}$ $-1.17^{+0.69}_{-0.68}, 14.38^{+2.31}_{-1.44}$	—	$10^{2.8} (/H0)$ $10^{2.4} (/H0)$
	$N_{\text{DW}} = 5$	✓		✓(full HD)	$-6.42^{+2.62}_{-1.41}, 14.30^{+1.61}_{-0.77}$ $-1.20^{+0.71}_{-0.79}, 14.29^{+2.28}_{-1.65}$	—	$10^{2.2} (/H0)$ $10^{1.8} (/H0)$
	$N_{\text{DW}} = 6$	✓		✓(full HD)	$-6.29^{+2.65}_{-1.48}, 14.38^{+1.64}_{-0.83}$ $-1.20^{+0.69}_{-0.82}, 14.30^{+2.29}_{-1.67}$	—	$10^{2.7} (/H0)$ $10^{2.1} (/H0)$
H3	$N_{\text{DW}} = 3$	✓	✓	✓(full HD)	$> -7.93, < 14.96$ $> -1.19, < 16.50$	$-14.73^{+0.71}_{-1.32}, 3.31^{+1.54}_{-1.72}, \text{—}$ $-14.63^{+0.67}_{-0.97}, 3.34^{+1.49}_{-1.67}, \text{—}$	$0.78 (/H1)$ $1.03 (/H1)$
	$N_{\text{DW}} = 4$	✓	✓	✓(full HD)	$> -7.97, < 15.12$ $> -1.22, < 16.51$	$-14.80^{+0.74}_{-1.52}, 3.28^{+1.62}_{-1.79}, \text{—}$ $-14.67^{+0.66}_{-0.99}, 3.41^{+1.47}_{-1.65}, \text{—}$	$0.81 (/H1)$ $1.01 (/H1)$
	$N_{\text{DW}} = 5$	✓	✓	✓(full HD)	$> -7.77, < 15.24$ $> -1.13, < 16.47$	$-14.70^{+0.76}_{-1.69}, 3.02^{+1.70}_{-1.73}, \text{—}$ $-14.63^{+0.65}_{-0.89}, 3.38^{+1.43}_{-1.62}, \text{—}$	$0.97 (/H1)$ $0.92 (/H1)$
	$N_{\text{DW}} = 6$	✓	✓	✓(full HD)	$> -7.96, < 14.88$ $> -1.15, < 16.53$	$-14.80^{+0.71}_{-1.33}, 3.43^{+1.49}_{-1.75}, \text{—}$ $-14.58^{+0.68}_{-1.09}, 3.18^{+1.57}_{-1.65}, \text{—}$	$0.82 (/H1)$ $0.98 (/H1)$
H4	$N_{\text{DW}} = 3$	✓	✓	✓(no-auto HD)	$> -8.02, < 14.76$ $> -0.83, < 16.52$	$-11.26^{+0.14}_{-0.17}, 0.54^{+0.42}_{-0.34}, \text{—}$ $-11.11^{+0.08}_{-0.13}, 0.34^{+0.37}_{-0.21}, \text{—}$	$0.57 (/H1)$ $0.90 (/H1)$
	$N_{\text{DW}} = 4$	✓	✓	✓(no-auto HD)	$> -8.15, < 14.55$ $> -0.85, < 16.46$	$-13.57^{+0.15}_{-0.14}, 4.50^{+0.31}_{-0.32}, \text{—}$ $-11.07^{+0.05}_{-0.09}, 0.65^{+0.27}_{-0.18}, \text{—}$	$0.63 (/H1)$ $0.88 (/H1)$
	$N_{\text{DW}} = 5$	✓	✓	✓(no-auto HD)	$> -8.08, < 14.53$ $> -0.77, < 16.31$	$-12.85^{+0.16}_{-0.16}, 2.23^{+0.35}_{-0.37}, \text{—}$ $-13.12^{+0.13}_{-0.13}, 3.62^{+0.32}_{-0.28}, \text{—}$	$0.57 (/H1)$ $0.87 (/H1)$
	$N_{\text{DW}} = 6$	✓	✓	✓(no-auto HD)	$> -8.02, < 14.83$ $> -0.96, < 16.40$	$-12.63^{+0.13}_{-0.12}, 2.91^{+0.28}_{-0.31}, \text{—}$ $-13.08^{+0.17}_{-0.16}, 3.87^{+0.38}_{-0.38}, \text{—}$	$0.68 (/H1)$ $0.88 (/H1)$
H5	✓		✓		—	$\text{—}, \text{—}, -14.89^{+0.10}_{-0.12}$	$10^{3.3} (/H0)$
H6	$N_{\text{DW}} = 3$	✓	✓	✓(full HD)	$> -7.93, < 14.74$ $> -0.90, < 16.47$	$\text{—}, \text{—}, -14.89^{+0.10}_{-0.12}$ $\text{—}, \text{—}, -14.92^{+0.11}_{-0.16}$	$0.72 (/H5)$ $0.88 (/H5)$
	$N_{\text{DW}} = 4$	✓	✓	✓(full HD)	$> -7.98, < 14.73$ $> -0.94, < 16.46$	$\text{—}, \text{—}, -14.94^{+0.13}_{-0.30}$ $\text{—}, \text{—}, -14.92^{+0.11}_{-0.16}$	$0.74 (/H5)$ $0.92 (/H5)$
	$N_{\text{DW}} = 5$	✓	✓	✓(full HD)	$> -8.02, < 14.69$ $> -0.94, < 16.44$	$\text{—}, \text{—}, -14.94^{+0.12}_{-0.29}$ $\text{—}, \text{—}, -14.93^{+0.12}_{-0.16}$	$0.71 (/H5)$ $0.90 (/H5)$
	$N_{\text{DW}} = 6$	✓	✓	✓(full HD)	$> -7.96, < 14.84$ $> -0.99, < 16.46$	$\text{—}, \text{—}, -14.94^{+0.12}_{-0.37}$ $\text{—}, \text{—}, -14.93^{+0.12}_{-0.18}$	$0.78 (/H5)$ $1.00 (/H5)$

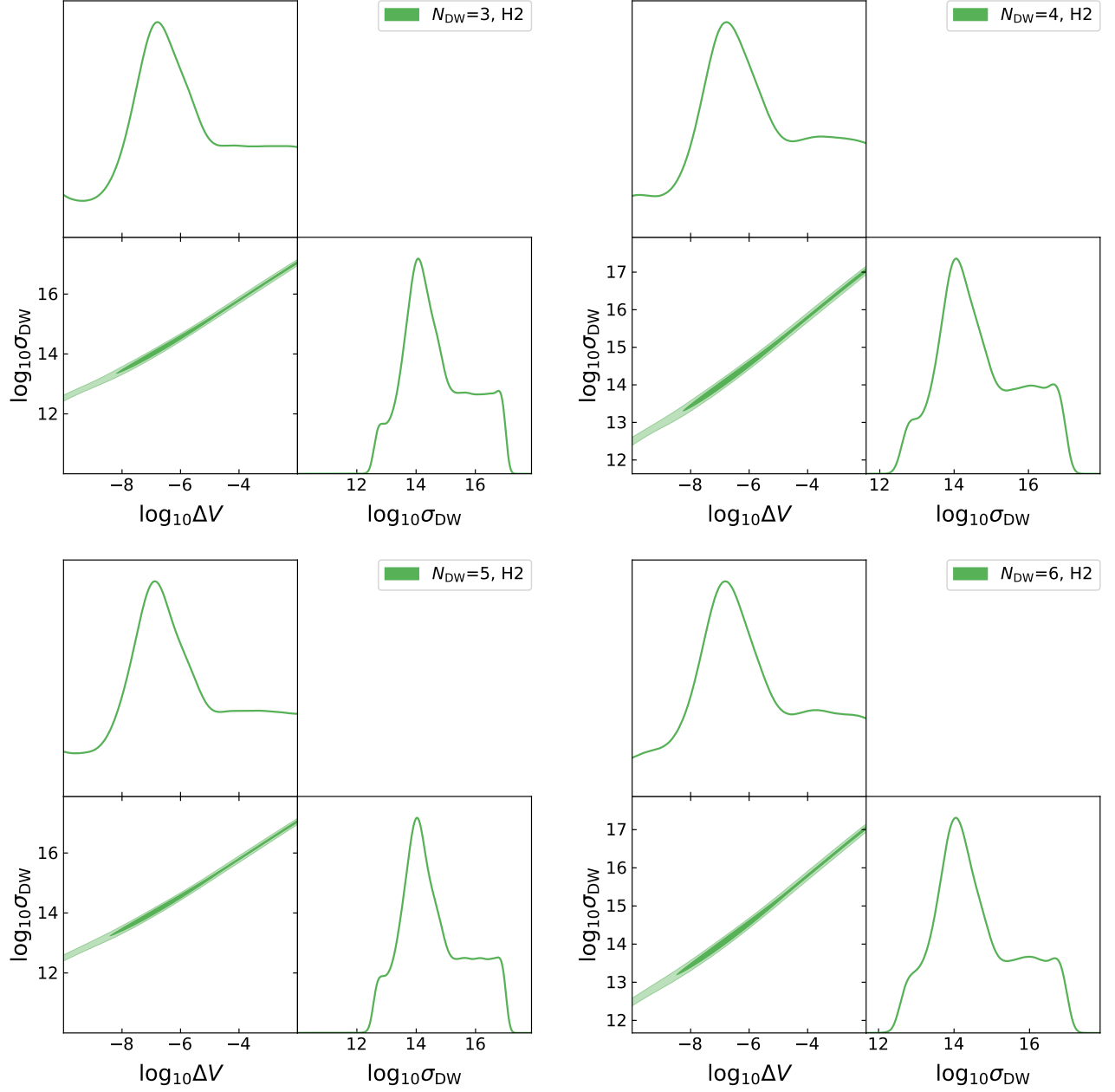


FIG. 5: Posterior distribution of the bias term $\log_{10}(\Delta V/\text{GeV}^4)$ and the wall tension $\log_{10}(\sigma_{\text{DW}}/\text{GeV}^3)$ with $N_{\text{DW}} > 2$ values for hypothesis H2 in Table IV.

2204.04228.

[36] M. F. Alam, Z. Arzoumanian, P. T. Baker, H. Blumer, K. E. Bohler, A. Brazier, P. R. Brook, S. Burke-Spolaor, K. Caballero, R. S. Camuccio, et al., The Astrophysical Journal Supplement Series **252**, 4 (2020), URL <https://doi.org/10.3847%2F1538-4365%2Fabc6a0>.

[37] B. B. P. Perera, M. E. DeCesar, P. B. Demorest, M. Kerr, L. Lentati, D. J. Nice, S. Osłowski, S. M. Ransom, M. J. Keith, Z. Arzoumanian, et al., Monthly Notices of the Royal Astronomical Society **490**, 4666 (2019), URL <https://doi.org/10.1093%2Fmnras%2Fstz2857>.

[38] M. Gonzalez, M. P. Hertzberg, and F. Rompineve, Journal of Cosmology and Astroparticle Physics **2020**, 028 (2020).

[39] H. Davoudiasl, Physical Review D **101**, 115024 (2020).

[40] K. V. Berghaus and T. Karwal, Physical Review D **101**, 083537 (2020).

[41] N. Aghanim, Y. Akrami, M. Ashdown, J. Aumont, C. Baccigalupi, M. Ballardini, A. J. Banday, R. B. Barreiro, N. Bartolo, S. Basak, et al., Astronomy & Astrophysics **641**, A6 (2020), ISSN 0004-6361, URL https://www.aanda.org/articles/aa/full_html/2020/09/aa33910-18/aa33910-18.htmlhttps://www.aanda.org/articles/aa/abs/2020/09/aa33910-18/aa33910-18.htmlhttps://www.aanda.org/

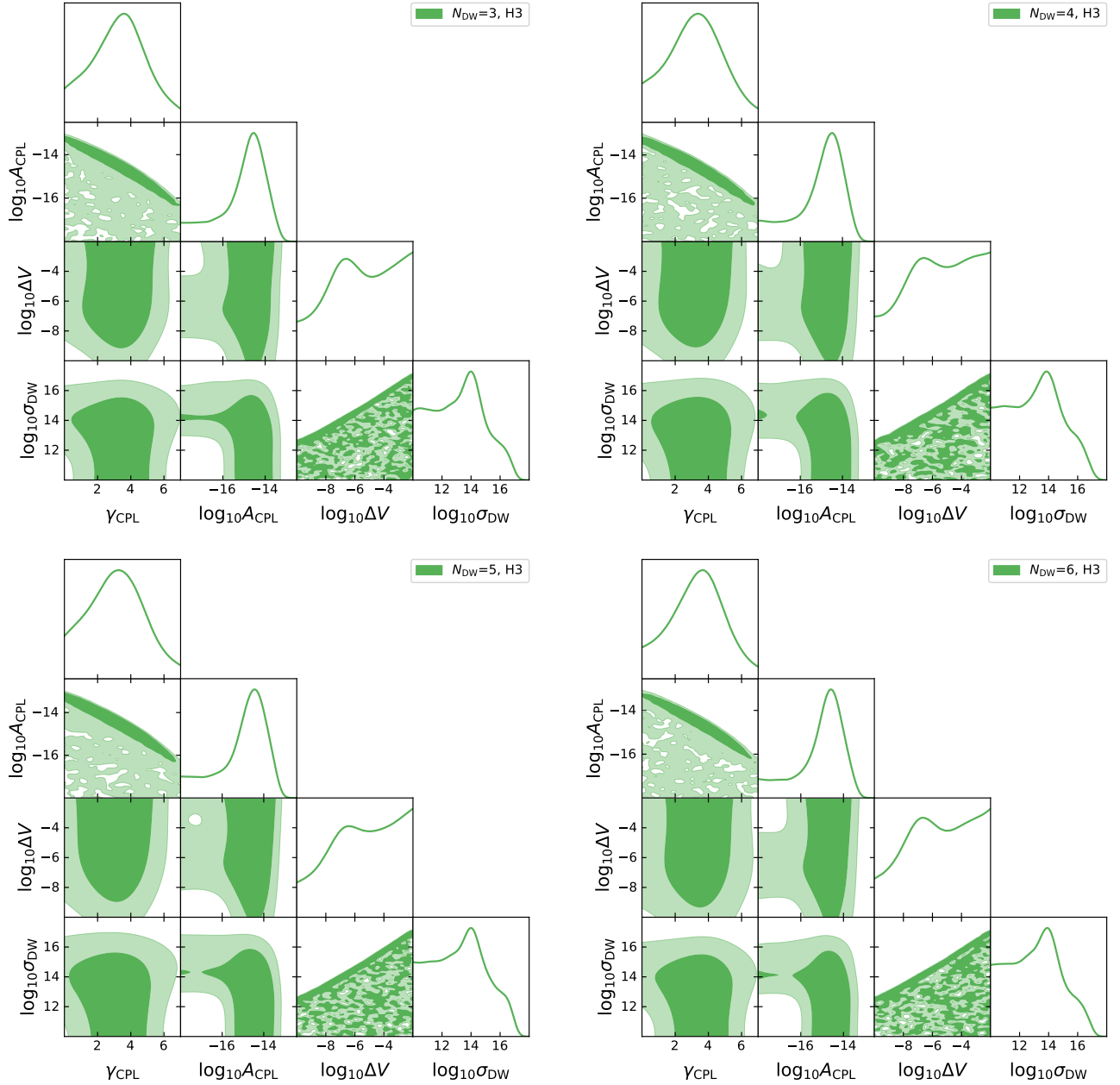


FIG. 7: Posterior distribution of the bias term $\log_{10}(\Delta V/\text{GeV}^4)$ and the wall tension $\log_{10}(\sigma_{\text{DW}}/\text{GeV}^3)$ with $N_{\text{DW}} > 2$ values for hypothesis H3 in Table IV.

- [org/10.1051/0004-6361/201833910](https://arxiv.org/abs/1807.06209)[http://arxiv.org/abs/1807.06209](https://arxiv.org/abs/1807.06209)[http://dx.doi.org/10.1088/1361-6382/ac086d](https://dx.doi.org/10.1088/1361-6382/ac086d)
- [42] A. G. Riess, S. Casertano, W. Yuan, J. B. Bowers, L. Macri, J. C. Zinn, and D. Scolnic, *The Astrophysical Journal Letters* **908**, L6 (2021).
- [43] N. Schöneberg, G. F. Abellán, A. P. Sánchez, S. J. Witte, V. Poulin, and J. Lesgourgues, *Physics Reports* **984**, 1 (2022).
- [44] E. Di Valentino, O. Mena, S. Pan, L. Visinelli, W. Yang, A. Melchiorri, D. F. Mota, A. G. Riess, and J. Silk, *Classical and Quantum Gravity* **38**, 153001 (2021), ISSN 0264-9381, URL <https://iopscience.iop.org/article/10.1088/1361-6382/ac086d><https://doi.org/10.1088/1361-6382/ac086d>
- [//iopscience.iop.org/article/10.1088/1361-6382/ac086d](https://iopscience.iop.org/article/10.1088/1361-6382/ac086d)[http://arxiv.org/abs/2103.01183](https://arxiv.org/abs/2103.01183)[http://dx.doi.org/10.1088/1361-6382/ac086d](https://dx.doi.org/10.1088/1361-6382/ac086d)
- [45] S. Vagnozzi, *Physical Review D* **102**, 023518 (2020), ISSN 24700029, URL <https://journals.aps.org/prd/abstract/10.1103/PhysRevD.102.023518>.
- [46] N. Blinov and G. Marques-Tavares, *Journal of Cosmology and Astroparticle Physics* **2020**, 029 (2020), ISSN 14757516, URL <https://iopscience.iop.org/article/10.1088/1475-7516/2020/09/029><https://iopscience.iop.org/article/10.1088/1475-7516/2020/09/029/meta>
- [47] K. Saikawa, *Universe* **3**, 40 (2017), URL <https://doi.org/10.3390/universe3040040>

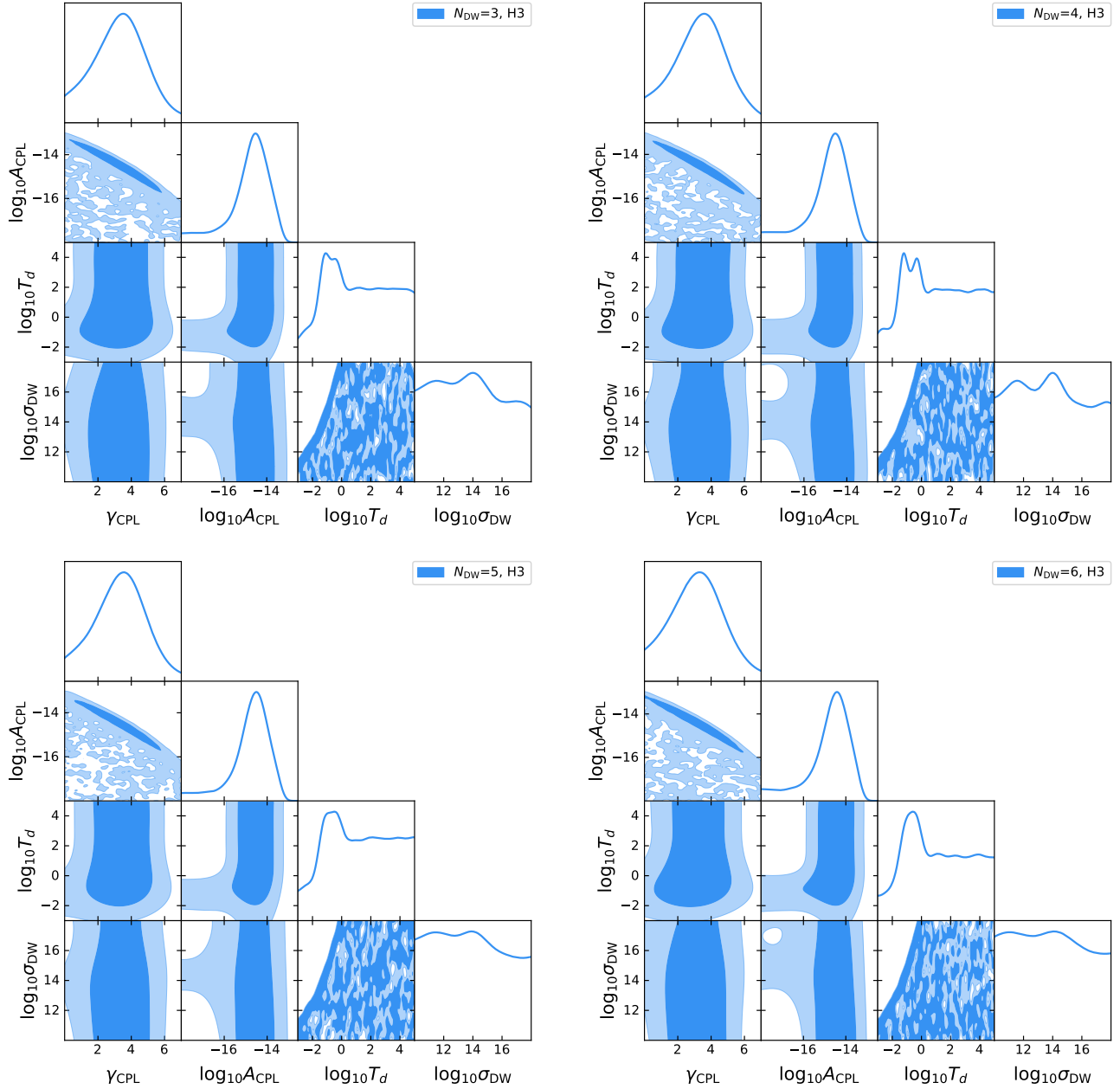


FIG. 8: Posterior distribution of the decay temperature $\log_{10}(T_d/\text{GeV})$ and the wall tension $\log_{10}(\sigma_{\text{DW}}/\text{GeV}^3)$ with $N_{\text{DW}} > 2$ values for hypothesis H3 in Table IV.

- 10.3390/Universe3020040.
- [48] S. Borsányi, Z. Fodor, J. Guenther, K.-H. Kampert, S. Katz, T. Kawanai, T. Kovacs, S. Mages, A. Pasztor, F. Pittler, et al., *Nature* **539**, 69 (2016).
 - [49] J. L. Ouellet, C. P. Salemi, J. W. Foster, R. Henning, Z. Bogorad, J. M. Conrad, J. A. Formaggio, Y. Kahn, J. Minervini, A. Radovinsky, et al., *Physical Review Letters* **122** (2019), URL <https://doi.org/10.1103/PhysRevLett.122.121802>.
 - [50] C. P. Salemi, J. W. Foster, J. L. Ouellet, A. Gavin, K. M. Pappas, S. Cheng, K. A. Richardson, R. Henning, Y. Kahn, R. Nguyen, et al., *Physical Review Letters* **127** (2021), URL <https://doi.org/10.1103/PhysRevLett.127.081801>.
 - [51] DMRadio Collaboration, L. Brouwer, S. Chaudhuri, H. M. Cho, J. Corbin, W. Craddock, C. S. Dawson, A. Droster, J. W. Foster, J. T. Fry, et al., *Dmradiom-3: A search for the qcd axion below 1 μev* (2022), URL <https://arxiv.org/abs/2204.13781>.
 - [52] A. Berlin, R. T. D'Agnolo, S. A. Ellis, and K. Zhou, *Physical Review D* **104** (2021), URL <https://doi.org/10.1103/PhysRevD.104.111701>.
 - [53] Z. Zhang, D. Horns, and O. Ghosh, *Physical Review D* **106** (2022), URL <https://doi.org/10.1103/PhysRevD.106.023003>.
 - [54] A. V. Gramolin, D. Aybas, D. Johnson, J. Adam, and A. O.

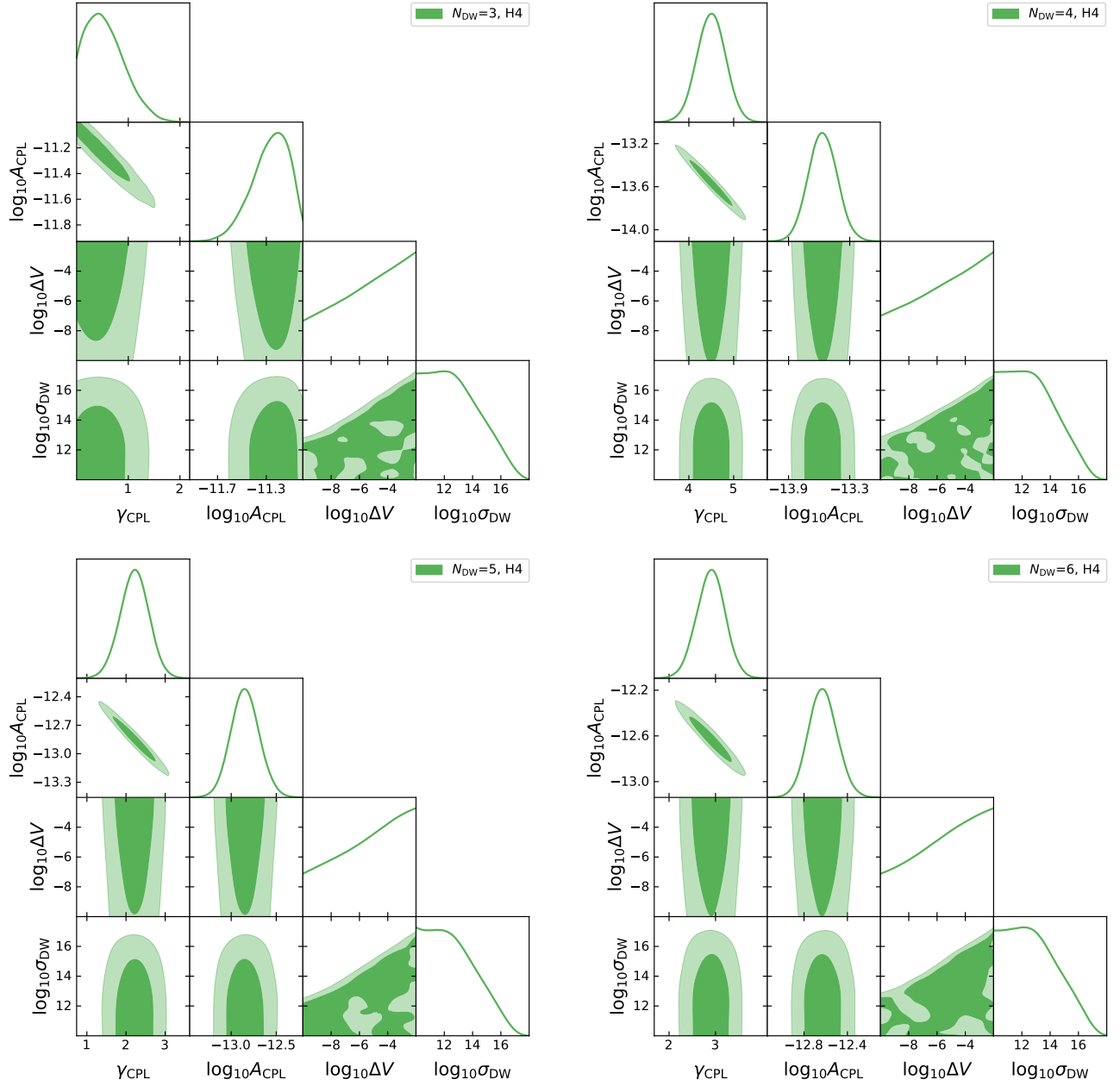


FIG. 9: Posterior distribution of the bias term $\log_{10}(\Delta V/\text{GeV}^4)$ and the wall tension $\log_{10}(\sigma_{\text{DW}}/\text{GeV}^3)$ with $N_{\text{DW}} > 2$ values for hypothesis H4 in Table IV.

- Sushkov, *Nature Physics* **17**, 79 (2020), URL <https://doi.org/10.1038/s41567-020-1006-6>.
- [55] D. F. Jackson Kimball et al., *Springer Proc. Phys.* **245**, 105 (2020), 1711.08999.
- [56] C. Li, *Phys. Rev. D* **102**, 123530 (2020), 2008.10264.
- [57] H. Murayama and J. Shu, *Phys. Lett. B* **686**, 162 (2010), 0905.1720.
- [58] S. Alam, M. Ata, S. Bailey, F. Beutler, D. Bizyaev, J. A. Blazek, A. S. Bolton, J. R. Brownstein, A. Burden, C.-H. Chuang, et al., *Monthly Notices of the Royal Astronomical Society* **470**, 2617 (2017).
- [59] A. J. Ross, L. Samushia, C. Howlett, W. J. Percival, A. Burden, and M. Manera, *Monthly Notices of the Royal Astronomical Society* **449**, 835 (2015).
- [60] F. Beutler, C. Blake, M. Colless, D. H. Jones, L. Staveley-Smith, L. Campbell, Q. Parker, W. Saunders, and F. Watson, *Monthly Notices of the Royal Astronomical Society* **416**, 3017 (2011).
- [61] D. M. Scolnic, D. Jones, A. Rest, Y. Pan, R. Chornock, R. Foley, M. Huber, R. Kessler, G. Narayan, A. Riess, et al., *The Astrophysical Journal* **859**, 101 (2018).
- [62] For topological defects formation during the phase transition through Kibble-Zurek mechanism and its connection with dark matter, see Ref. [57].

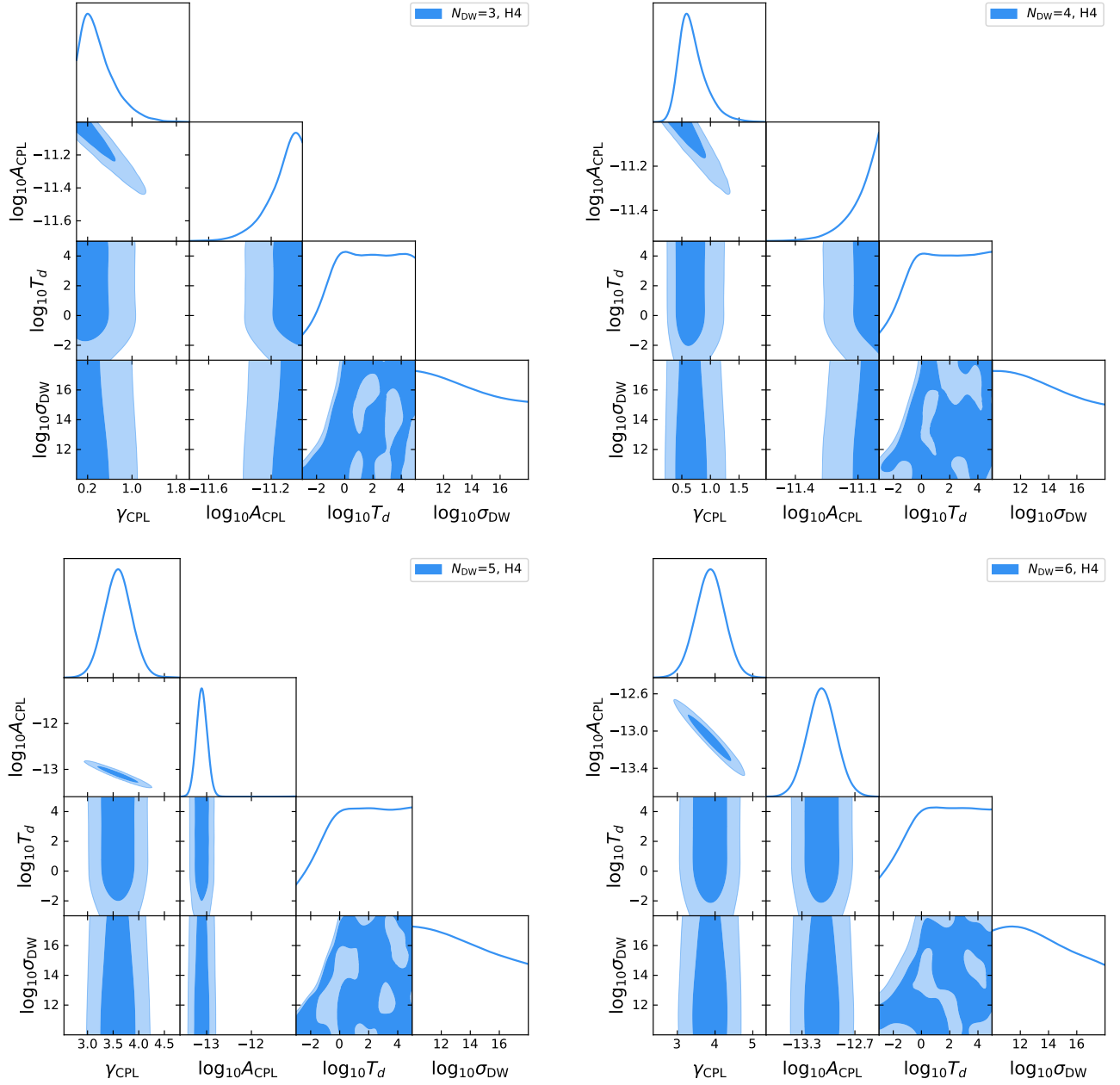


FIG. 10: Posterior distribution of the decay temperature $\log_{10}(T_d/\text{GeV})$ and the wall tension $\log_{10}(\sigma_{\text{DW}}/\text{GeV}^3)$ with $N_{\text{DW}} > 2$ values for hypothesis H4 in Table IV.

- [63] Refs. [4, 5] have numerically simulated in detail the generation of GWs by DW networks with different N_{DW} based on QCD axion model and $\lambda\phi^4$ model. But their result is quite general as the shape of the DW-induced GWs is primarily model-independent.
- [64] <https://doi.org/10.4225/08/5aff8174e9b3>
- [65] <https://github.com/nanograv/enterprise>
- [66] https://github.com/nanograv/enterprise_extensions

- [67] Different choices of datasets can reduce the Hubble tension to different levels. Here, the 2.7σ tension is obtained by fitting to the dataset of *Planck 2018 + CMB lensing* [41] with a freely-varying self-interacting ΔN_{eff} . The tension would be reduced to 2.9σ [46] with *BAO* data [58–60] included and 3.2σ [43] with *Pantheon* data [61] further included.

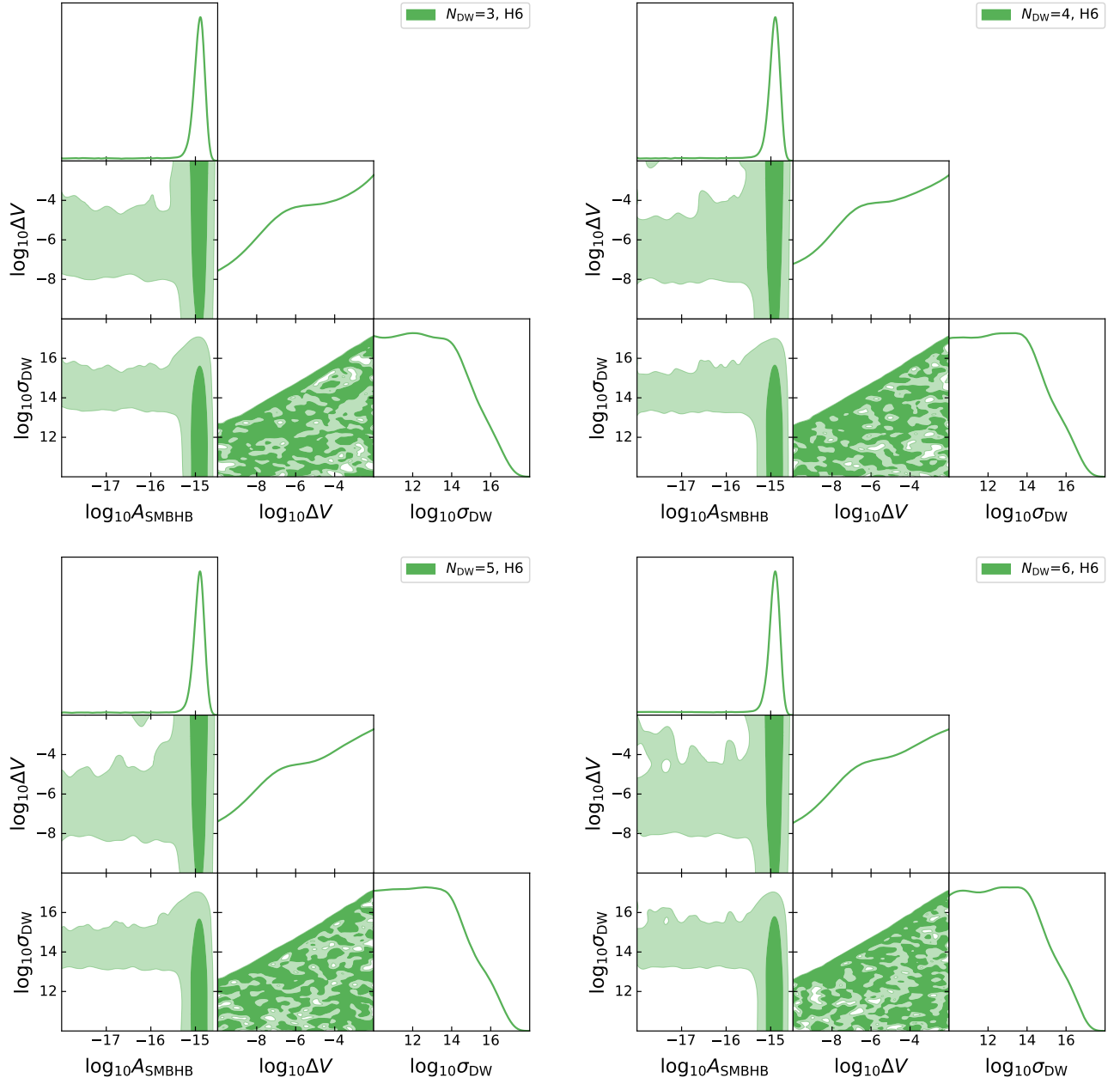


FIG. 11: Posterior distribution of the bias term $\log_{10}(\Delta V/\text{GeV}^4)$ and the wall tension $\log_{10}(\sigma_{\text{DW}}/\text{GeV}^3)$ with $N_{\text{DW}} > 2$ values for hypothesis H6 in Table IV.

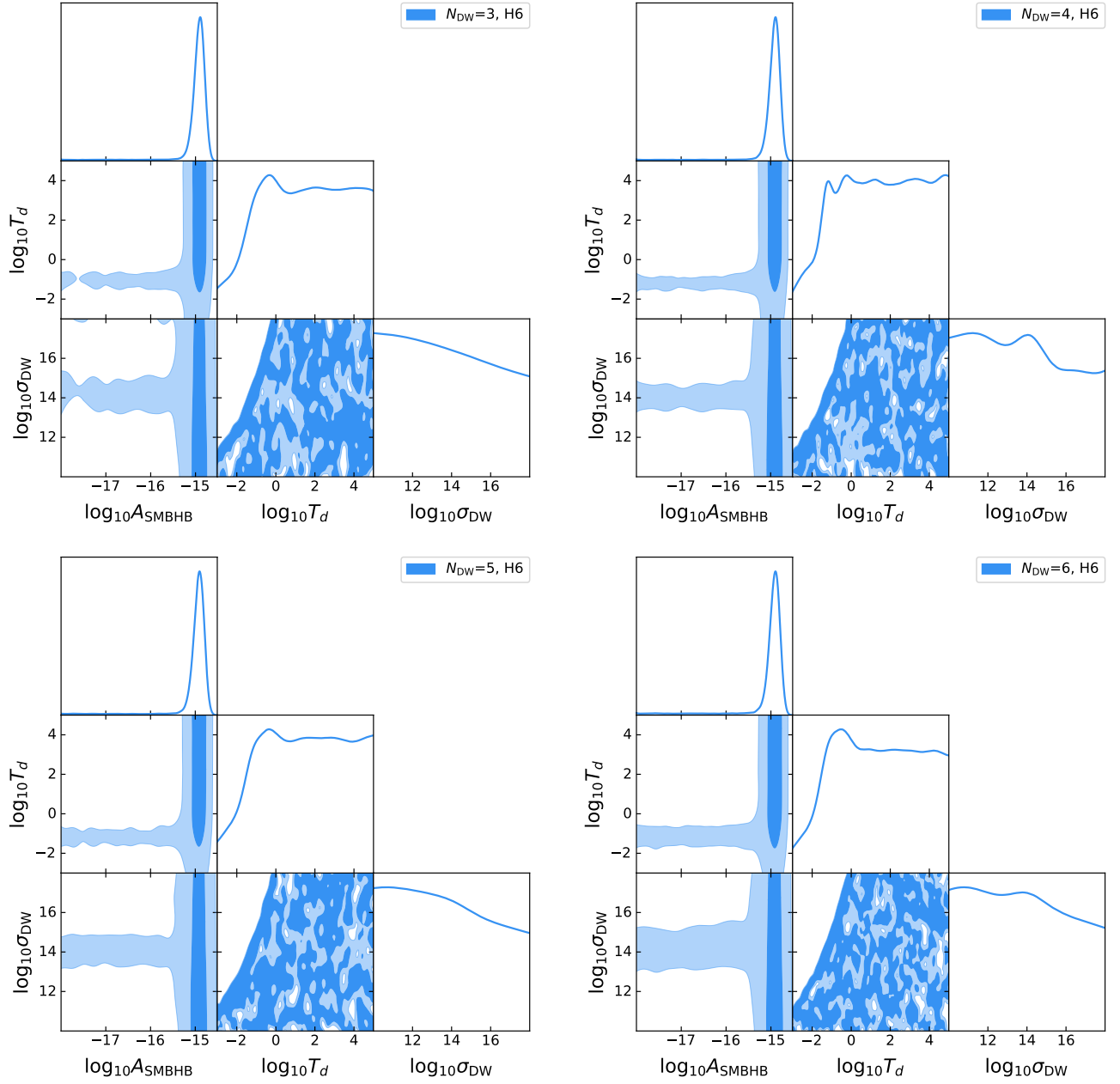


FIG. 12: Posterior distribution of the decay temperature $\log_{10}(T_d/\text{GeV})$ and the wall tension $\log_{10}(\sigma_{\text{DW}}/\text{GeV}^3)$ with $N_{\text{DW}} > 2$ values for hypothesis H6 in Table IV.

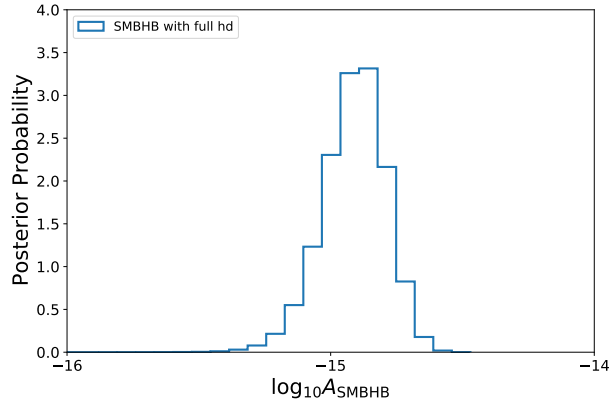


FIG. 13: Posterior distribution of A_{SMBHB} of the H5 case in the Table IV.